



Universiteit
Leiden
The Netherlands

High-dimensional profiling of immunotherapy-responsive immune cells in cancer

Beyrend, G.

Citation

Beyrend, G. (2021, June 8). *High-dimensional profiling of immunotherapy-responsive immune cells in cancer*. Retrieved from <https://hdl.handle.net/1887/3185499>

Version: Publisher's Version

License: [Licence agreement concerning inclusion of doctoral thesis in the Institutional Repository of the University of Leiden](#)

Downloaded from: <https://hdl.handle.net/1887/3185499>

Note: To cite this publication please use the final published version (if applicable).

Cover Page



Universiteit Leiden



The handle <https://hdl.handle.net/1887/3185499> holds various files of this Leiden University dissertation.

Author: Beyrend, G.

Title: High-dimensional profiling of immunotherapy-responsive immune cells in cancer

Issue Date: 2021-06-08

DISCOVERY OF CIRCULATING
EFFECTOR T CELL STATES
CONNECTED TO EFFECTIVE
IMMUNE CHECKPOINT THERAPY

5

ABSTRACT

Immune checkpoint therapy (ICT) has the potency to eradicate cancer but the characteristics and mechanisms of effective *versus* non-effective therapy-induced immune responses remain to be elucidated. Here, using high-dimensional single-cell profiling we define T cell states that develop in response to effective ICT eradicating syngeneic mouse tumors. Unbiased assessment of transcriptomic alterations of therapy-responsive T cells in the circulation by single-cell RNA sequencing and system-wide profiling of cell-surface protein expression by mass cytometry revealed unique effector CD4⁺ and CD8⁺ T cell states. The therapy-responsive CD4⁺ and CD8⁺ effector T cells displayed distinct NK cell receptors and chemokine receptors, and these cells were system-wide existing. Functional targeting of these molecules in tumor-bearing mice showed their functional importance for therapy-induced anti-tumor immunity. Moreover, NK cell receptor-expressing effector T cells were also present in the peripheral blood of immunotherapy-responsive cancer patients. These findings provide a better understanding of ICT and highlight the use of biomarkers on effector CD4⁺ and CD8⁺ T cells to improve cancer immunotherapy.

Manuscript in preparation

Guillaume Beyrend¹, Esmé T.I. van der Gracht^{1*}, Tetje C. van der Sluis^{1*}, Tamim Abdelaal^{2,3}, Simon Jochems⁴, Bob Belderbos⁵, Tom Wesselink¹, Suzanne van Duikeren¹, Anke Redeker¹, Elham Beyranvand Nejad⁶, Marcel Camps¹, Adriaan Bins⁷, John BAG Haanen⁸, Joachim G Aerts⁵, Ferry Ossendorp¹, Ramon Arens¹

¹ Department of Immunology, Leiden University Medical Center, Leiden, The Netherlands

² Pattern Recognition and Bioinformatics, Delft University of Technology, Delft, The Netherlands

³ Leiden Computational Biology Centre, Leiden University Medical Centre, Leiden, The Netherlands

⁴ Department of Parasitology, Leiden University Medical Centre, Leiden, The Netherlands

⁵ Department of Pulmonary Diseases, Erasmus Medical Center, Rotterdam, The Netherlands

⁶ Department of Medical Oncology, Leiden University Medical Centre, Leiden, The Netherlands

⁷ Department of Department of Medical Oncology, Amsterdam UMC, location AMC, Amsterdam, the Netherlands.

⁸ Division of Molecular Oncology and Immunology, Netherlands Cancer Institute, Amsterdam, the Netherlands

*shared authorship

INTRODUCTION

Immunotherapy has become an important treatment against cancer, but a deeper understanding of factors governing immune responses in cancer is required to extend clinical efficacy to the majority of patients. Many studies have focused on profiling intratumoral CD8 T⁺ cells, however recent studies have demonstrated that systemic anti-tumor immune responses are essential for immunotherapeutic efficacy (1). A comprehensive description of how immunotherapy during cancer development affects the systemic T cell states is lacking.

Regression of solid tumors is generally positively correlated with T cells infiltrating the tumor tissue (2). Expression of inhibitory molecules including PD-1 and CTLA-4 on these T cells, however, associate with impaired function such as diminution of the cytotoxic and proliferative potential (3). To counteract the cancer-associated T-cell inhibition, successful therapies were developed that were able to antagonize such T-cell inhibition leading to durable responses (4, 5). This type of immunotherapy, named immune checkpoint therapy (ICT), provides currently an established treatment option for several types of cancer. However, long-term survival can only be achieved in a minority of patients, which warrants to determine the probability of clinical response rates and the development of more efficacious treatment options. In this respect, a better understanding of the cellular mechanisms that mediate tumor rejection could support both the clinical prospects as the design of optimal treatment modalities (6). Non-invasive screening methods with predictive biomarkers related to effective therapy are highly desired, especially, in light of the many clinical trials that incorporate novel (combinatorial) immunotherapeutic approaches that are on-going (7).

The application of single-cell RNA sequencing (sc-RNA-seq) to cancers has provided unprecedented insights into the tumor microenvironmental heterogeneity. Deep immunophenotyping using other single-cell technologies such as high-dimensional cytometry has also been instrumental in understanding how the tumor micro-environment was shaped upon immunotherapy (8-10). For example, by using these single-cell technologies it was shown that the intratumoral T cells have different states of functionality ranging from functional cytotoxicity to exhausted states. Cancer immunity has also been investigated on a systemic level, showing key roles for T cells, NK cells (11), monocytes (12) and macrophage (13) subsets (14-16).

In this study, we analyzed the T cell response to different types of immunotherapeutic regimens, representing different response levels of the immune system towards murine tumors. We used two forms of high-dimensional single-cell profiling—single-cell RNA sequencing (17) and mass cytometry (CyTOF) (18)—to assess transcriptional and proteomic changes of responding T cell populations. We found specific effector T cell subsets in the blood, characterized by specific biomarkers (e.g. transcription factors, chemokines and NK cell markers), which connected functionally to the treatment and the related tumor rejection. System-wide analysis revealed that the therapy-responsive T

1

2

3

4

5

6

7

&

cells were not limited to the blood but connected to other main immune compartments like the spleen, bone marrow and lymph nodes. Finally, we extrapolated the results to human settings by analyzing peripheral blood mononuclear cells shortly after therapy, and found T cell states in the blood that correlated with the clinical response rate. Together, this study reveals heretofore unrecognized dynamic cellular changes occurring during ICT, and the role of a set of biomarkers, which are of importance in tumor immunity and could be used in screening to assess the level of immunotherapy efficiency.

MATERIALS AND METHODS

Mice and tumor cell lines

C57BL/6 female mice were obtained from Janvier Laboratories (Le Genest-Saint-Isle, France). At the start of the experiments, mice were 6 to 8 weeks old. $Spn^{-/-}$ mice ($Spn^{em1Lumc}$) on a C56BL/6 background were generated using CRISPR-Cas9-mediated targeting of zygotes, which resulted in deletion of the coding sequence of Exon 2 of the *Spn* (Cd43) gene. Mice were housed in individually ventilated cages (IVC) under specific pathogen-free (SPF) conditions in the animal facility of Leiden University Medical Centre (LUMC, The Netherlands). All mouse experiments were controlled by the animal welfare committee (IvD) of the Leiden University Medical Center and approved by the national central committee of animal experiments (CCD) under the permit number AVD116002015271, in accordance with the Dutch Act on Animal Experimentation and EU Directive 2010/63/EU.

Tumor challenge models

Treatment schedule of experiments are indicated in the respective figures and legends. In tumor experiments, mice were inoculated in the flank with 0.3×10^6 MC-38 (subcutaneously) or HCMel12 (intra-dermally) tumor cells in respectively 200 μ L or 30 μ L PBS containing 0.2% BSA on day 0. Tumor outgrowth was measured by caliper in three dimensions, until mice had to be sacrificed due to tumor burden, according to local ethical guidelines. Briefly, mice were euthanized when tumor size reached 1000 mm^3 in volume or when mice lost over more than 20% of their total body weight (relative to initial body mass).

In vivo antibody usage

OX40 (clone OX86) was injected subcutaneously next to the tumor together with anti-CpG 6 days after tumor inoculation to agonistically target OX40 and CpG. α PD-L1 (clone MIH5) blocking antibodies were administered intraperitoneally 10, 13 and 16 days after tumor inoculation.

CD4⁺ (clone GK1.5) and CD8⁺ (clone 2.43) T cell depleting monoclonal antibodies were produced in the LUMC and administered intraperitoneally twice weekly (respectively 150 μ g/mouse first injection followed by 150 μ g/mouse injections) for 2 weeks. CD8⁺ T

cell depletion was started 4 days before tumor challenge. Depletion was checked by staining for CD3, CD4 and CD8 marker expression followed by flow cytometric analysis.

CXCR3 and NKG2D depleting antibodies were purchased from BioXCell and administered intraperitoneally three times a week for a total of 4 injections. Correct blocking of CXCR3 and NKG2D receptors was verified by flow cytometry using CXCR3 and NKG2D antibodies in the antibody mix presented in Figure S1 and used in Figure 4.

MACS sorting and debris removal

To purify mouse T cells extracted from the blood, the Pan T Cell Isolation Kit I for mouse (130-095-130, Miltenyi Biotec) was used two consecutive times to reach a high level of T cell purity, consequently check by flow cytometry after blood lysis step. A consecutive step to remove debris from the blood was performed by using the Debris Removal Solution (130-109-398) from Miltenyi Biotec according to the manufacturer protocol. Results by flow cytometry (7AAD, CD4 - FITC, CD8 -APC, CD3 -BV510) showed a purity of more than 95% (data not shown) and was then sequenced for single-cell-RNA-sequencing.

Organ processing

Tumor-bearing mice were sacrificed, and transcardially perfused with 30 mL of PBS/EDTA (2 mM) to eliminate blood contamination of tumor material mainly. Tumors were minced, incubated with 2.5 mg/mL Collagenase D and DNase (Roche) for 20 minutes at 37°C and single-cell suspensions were made using 70- μ m cell strainers (BD Biosciences). For further processing with mass cytometry, tumor infiltrating lymphocytes were purified with a 40/60/80/100 Percoll (GE Healthcare) gradient. Spleen and lymph nodes were minced through a 70- μ m cell strainers, bone marrow was extracted from the bones by flushing with medium 8% FBS. On all samples, red blood cells were lysed for 2 minutes with a lysis buffer. Samples were then washed with medium 8% FBS and analyzed by flow or further processed for analysis by mass cytometry.

Flow cytometry analysis

Samples obtained from the organ processing steps were rinsed with flow cytometry buffer (PBS with 2% FBS). Mouse Fc-Receptors were blocked with anti-mouse CD16/32 (clone 2.4G2) and 10% naïve mouse serum for 15 minutes before antibody staining. Cells were then stained using combinations of antibodies as shown in Figure S1. Samples were acquired on a Fortessa (BD) and analyzed using FlowJo software (Tree Star).

Mass cytometry (CyTOF)

Single cell suspensions of mouse tumors were prepared identically as for flow cytometry, as described above. In addition, debris, tumor cells and aggregates were removed using a 100/60/40/30-percent gradient of Percoll (GE HealthCare) in RPMI 1640 (Lonza), resuspending pelleted single cells in the 40% fraction. This procedure did not skew

1

2

3

4

5

6

7

&

the abundance of macrophage subsets as assessed by flow cytometry of the same tumor samples with and without using the Percoll gradient (data not shown). Approximately 3 million cells were then taken for antibody staining. Metal-conjugated antibodies were purchased from Fluidigm Sciences, other antibodies were conjugated in-house using the MaxPar X8 antibody labeling Kit (Fluidigm Sciences) according to manufactures instructions. For all non-cadmium metals or with the Maxpar MCP9 for cadmium metals, and respectively stored in Antibody Stabilization Buffer (Candor Bioscience GmbH) or HRP-Protector™ peroxidase stabilizer (Boca Scientific) was used.

Mass cytometry staining

All reagents were purchased from Fluidigm Sciences unless stated otherwise. In short, samples were incubated with 1 μM Cell-ID intercalator-103Rh to identify dead cells, followed by blockage of mouse serum (2%) and Fc blocking anti-mouse CD16/32 (clone 2.4G2, BD Biosciences: 5%). Then, the metal-conjugated antibody mix was added, and cells were incubated overnight up to 48 hours with 125 nM Cell-ID Intercalator-Ir in MaxPar Fix and Perm. Prior to acquisition on a Helios mass cytometer, samples were centrifuged and resuspended in MilliQ and measured directly. Data were normalized using EQ Four Element Calibration Beads with the reference EQ passport P13H2302. Data analysis was performed by pre-gating live singlet CD45⁺ cells using FlowJo software (Tree Star), followed by non-supervised clustering based using the hierarchical t-SNE (HSNE) function of Cytosplore with 5 levels.

Single-Cell RNA Sequencing Library Generation

Droplet-based 3' end massively parallel single-cell RNA sequencing (scRNAseq) was performed by encapsulating sorted live CD45⁺ tumor infiltrating cells into droplets and libraries were prepared using Chromium Single Cell 3' Reagent Kits v1 according to manufacturer's protocol (10x Genomics). The generated scRNAseq libraries were sequenced using an Illumina HiSeq2500.

Preprocessing Analysis with Seurat Package

Downstream analysis was performed using the Seurat R package (34). Briefly, for each sample (OX40, PDL1, PDOX and untreated), mitochondrial, ribosomal and hemoglobin genes were excluded. Further, cells expressing less than 200 genes, and genes that were expressed in less than 3 cells were excluded. Next, all samples were pooled together into one dataset, and outlier cells expressing more than 2900 genes were excluded, which resulted in a dataset of 5260 cells. Next, the dataset was log_{1p} normalized with a scaling factor of 10,000. Next, the set of 1709 highly variable genes were selected for further analysis. Dataset was preprocessed using principal component analysis. Using the top 15 principle components, the dataset was clustered using Louvain (graph-based community detection) and visualized using tSNE (35). Differentially expressed genes (DEgenes) were

identified between different cell groups, using Wilcoxon rank sum test with Bonferroni multiple test correction. DEgenes were visualized using violin plots, where statistically significant genes had adjusted P-value < 0.05. Within the CD4⁺ and CD8⁺ T cells separately, cells expressing the Cxcr3, Klrk1 and Klrc1 genes were compared. DE genes were obtained between positive and negative groups of cells expressing these genes (expression > 1 was considered positive, otherwise negative).

Statistics

All *in vivo* and *ex vivo* data are presented as mean and SEM unless stated otherwise. Statistical comparison of groups was performed using an ANOVA and unpaired two-tailed Student's t test (two-tailed). A minimum of three biological replicates was used in all experiments, as specified in figure legends. Differences were considered statistically significant at *p* < 0.05.

RESULTS

Identification of circulating immunotherapy-responsive T cell subsets by sc-RNA-seq

To analyze T cell states associated with efficient immune checkpoint therapies, we challenged wild-type mice with syngeneic MC38 colorectal tumors (19), and then treated tumor-bearing mice with αPD-L1 antibody, blocking the inhibitory checkpoint pathway PD-1/PD-L1, and with agonistic antibodies stimulating the costimulatory receptor OX40 on tumor-specific T cells (Figure 1A). The blockade of the PD-1-PD-L1 axis resulted in delayed tumor outgrowth and cure in 30% of the mice, whereas anti-OX40 treatment resulted in a non-significant delay of tumor outgrowth. However, addition of the TLR9 ligand CpG augmented the antitumoral actions of anti-OX40 (Figure S1), which is in line with a previous report (20). Strikingly, the combination of αPD-L1 blockade and anti-OX40/CpG induced cure in the majority of mice (Figure 1B). The combination of the two immunotherapeutics (αPD-L1 and anti-OX40/CpG), referred hereafter as PDOX, was correspondingly most effective against established syngeneic HCMel12 melanoma tumors (21) (Figure 1C).

To identify circulating T cell subsets that respond to effective checkpoint therapy, we isolated CD4⁺ and CD8⁺ T cells from the peripheral blood at day 18 post tumor challenge. Per condition >1,000 cells were analyzed by single-cell RNA sequencing (sc-RNA-seq) with a coverage of 60,000 reads per cell. The subpopulation structure of the circulating T cells was defined by pooling data from the different treatment groups representing 5,600 cells total and using the Seurat package analysis to identify transcriptional clusters (Figure 1D, Figure S2B). Six distinct T cell clusters could be identified consisting of three CD4⁺ and three CD8⁺ T cell clusters (Figure 1E). Two clusters (CD4-T3, CD8-T3) were over-represented in the PDOX group (Figure 1F), and these clusters were characterized by *Id2* and *Lgals1* transcripts encoding for the transcription factor ID2 and Galectin-1,

1

2

3

4

5

6

7

&

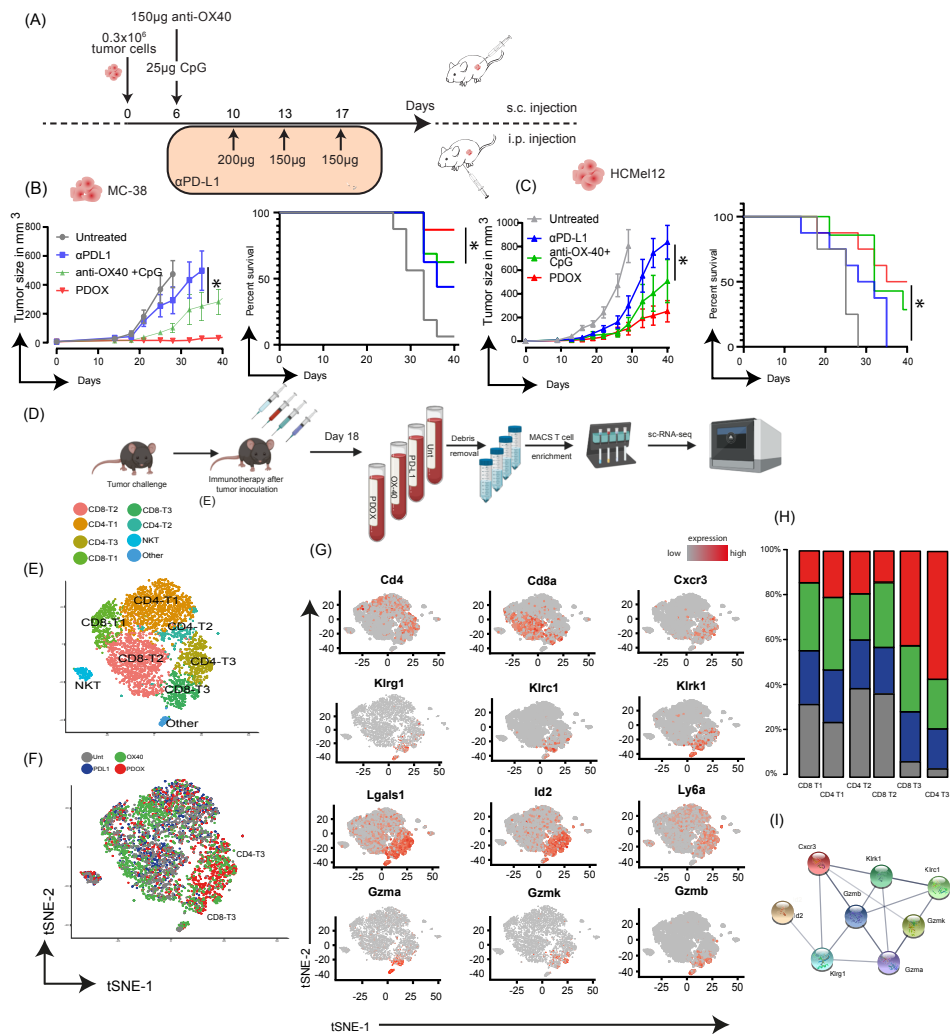


Figure 1. Synergy of immunotherapy targeting inhibitory and activating immune checkpoints. (A) Schematic summary of the therapy regimen. (B) Left panel: comparison of mean (\pm SEM) of MC38 tumor growth between the untreated (grey), OX40 + CpG (green), PD-L1 (blue), combination PDL1 and OX-40, named PDOX group (red), $n=16$ mice per group. Right panel: Survival of MC38-tumor bearing mice (C) Same as in (B), HCMel12 tumor, $n=8$ mice per group. (D) Protocol of blood isolation on tumor-bearing mice receiving immunotherapy or left untreated meant for sc-RNA-sequencing analysis. One mouse from each group are submitted to the same antibody regimen as explained in (B). 18 days after tumor inoculation, mice are sacrificed, blood is collected and purified for its T cell compartment using MACS separation. Cells are then sequenced by 10X Genomics Reader. (E) tSNE plot of cells color coded by identified subsets (F) Same as in (E), color coded by group, as explained in (B). (G) Same as in (E) color coded by the expression of the relative gene (Cd4, Cd8a, Cxcr3, Klr1, Klrg1, Klrc1, Klrc1, Lgals1, Id2, Ly6a, Gzma, Gzmk, Gzmb) from grey to red. (H) Bar graph representing the percentage of all the 6 subsets according to their group (Untreated in grey, PD-L1 in blue, OX40 in green or PDOX in red).

respectively (Figure 1G). Other gene transcripts overrepresented in both CD4-T3 and CD8-T3 cells were *Cxcr3* (coding for the chemokine receptor CXCR3) and *Ly6a* (coding for Sca-1). Transcripts linked to NK cell markers and cytotoxicity including *Klrc1* (coding for NKG2D protein), *Klrc1* (coding for NKG2A), *Klrg1* (coding for KLRG1), *Nkg7* (coding for NKG7), *Ccl5* (coding for CCL5), *Gzma*, *Gzmb*, and *Gzmk* (coding for Granzyme A, B, K) were enriched in CD8-T3 (Figure 1H). *Klrc1* and *Klrc1* transcripts were also found in the CD4-T3 cluster. The upregulated genes upon combination therapy are linked to each other, highlighting the *Klr* relationship evolving around cytotoxicity power (Figure 1I).

Transcriptional profiling of immunotherapy-responsive T cell subsets

The CD4-T3 and CD8-T3 clusters were characterized by a high level of *Id2* transcripts (Figure 2A), and this connected closely to *Lgals1* transcripts (Figure S2B). To search for cell-surface markers associated with these genes we identified the effector T cell-associated glycoform of sialoforine (CD43) using the 1B11 mAb, given the association of ID2 with effector T cell formation (22) and of the association of Galectin-1 with different CD43 glycoforms (23). The antibody clone S11, recognizing CD43 regardless of glycosylation, was not useful in this respect as it identifies CD43 expression on virtually on all T cells being activated or not (Figure S3). Strikingly, the majority of the ID2⁺ CD8⁺ T cells expressed the hyperglycosylated CD43 isoform while only a minority of the ID2⁺ CD8⁺ T cells expressed this CD43 isoform (Figure 2B), and similar results were found for CD4⁺ T cells (data not shown). Moreover, CD43 positivity correlates closely to PDOX treatment (Figure 2C).

To functionally test whether CD43 is implicated in the efficacy of effective checkpoint therapy, we challenged mice deficient in the *Spn* gene (coding for CD43) with MC38 tumor cells, and treated these mice with PDOX. Whereas CD43 proficient mice showed therapeutic efficacy of PDOX upon tumor challenge, the mice deficient in CD43 could not control MC38 tumors despite PDOX treatment (Figure 2D). Moreover, PDOX treatment efficacy was highly dependent on CD8⁺ T cells (Figure 2E), suggesting that mainly the effector-type CD8⁺ T cells characterized by the activation-associated glycoform of CD43 are crucial. In line with this, an increased percentage of CD43⁺CD8⁺ T cells was found in blood and tumors upon PDOX treatment (Figure 2F). Furthermore, the vast majority of tumor-specific CD8⁺ T cells recognizing the neoantigen *Adpgk* expressed by MC38 tumors, were positive for CD43 (Figure 2G).

To accurately define the signature of the circulating CD43⁺CD8⁺ and CD43⁺CD4⁺ T cells subsets we performed bulk mRNA sequencing on FACS sorted CD43⁻ and CD43⁺ T cells from tumor-challenge PDOX treated mice. The circulating CD43⁺CD8⁺ and CD43⁺CD4⁺ T cells had overlapping gene signatures as the genes expressed in the CD4-T3 and CD8-T3 clusters (e.g. *Id2*, *Lgals1*, *Klrc1*, *Klrg1*, *Klrc1*, *Ly6a*, *Cxcr3*, *Gzmb*) as detected by single cell RNA sequencing (Figure 2H).

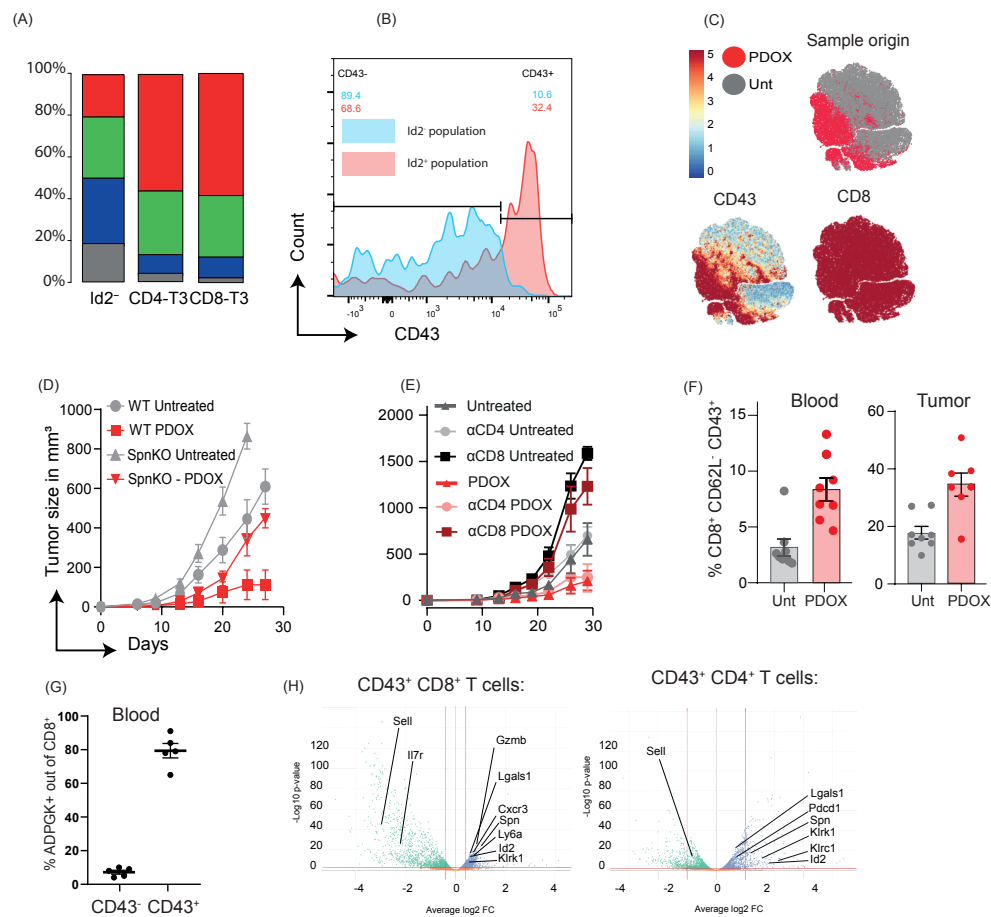


Figure 2. Transcriptional profiling identifies unique effector CD4 and CD8 T cell subsets enriched during effective immunotherapy. Bar graph representing the cell origin per group: untreated (grey), PD-L1 (blue), OX-40 (green), PDOX (red). Representative flow cytometry plot of an ID2⁻ and ID2⁺ population regarding their CD43 expression from a PDOX treated mouse. tSNE plots of flow cytometry data shown per sample group (untreated in grey and PDOX in red), or by the CD8 and CD43 expression (in a blue-to-red scale). Histograms showed a higher expression of CD43 on combined treatment group (mean represented, n=8 samples per group). Average of tumor growth of wild type tumor mice (WT Untreated, round grey), wild type mice receiving PDOX treatment (WT PDOX, square red) Spn^{-/-} mice untreated (SpnKO Untreated, triangle grey) and Spn^{-/-} treated with combination of antibodies (SpnKO - PDOX, triangle red), n=8 mice per group. Average of tumor growth of wild type mice (Untreated, triangle grey), CD4 depleted mice untreated (αCD4 Untreated, grey circle), CD8 depleted mice untreated (αCD8 Untreated, black square), wild type mice treated with PDOX treatment (red, triangle), CD4 depleted mice treated with PDOX treatment (αCD4 PDOX, pink circle), CD8 depleted mice treated with PDOX treatment (αCD8 PDOX, dark red square). Histogram showing the difference of CD8⁺ CD62L⁻ CD43⁺ % in blood and tumor between untreated (Unt) and combination group (PDOX). Proportion of ADGK⁺ cells in blood which are CD43⁻ or CD43⁺. Bulk RNA-seq experiments of sorted CD43⁺ CD8⁺ T cells and CD43⁺ CD4⁺ T cells from wild type mice treated after 8 days of PDOX treatment.

Functional characterization of immunotherapy-responsive T cell subsets

A subset of the CD43⁺ T cells exhibited NK cell-associated gene expression including *Klkr1* and *Klrc1*. These genes are key molecules related to the effector capacity of NK cells as well as T cells. In the CD8⁺ lineage, the *Klkr1*⁺ cells associated to expression of other *Klr* family receptors (*Klrc1*, *Klrc2*, *Klre1*), to the metabolic receptors *Lgals1* and *Lgals3*, to the chemokine ligand *Ccl5* and to chemokines receptor *Cxcr3*. These cells also expressed *Granzyme A* and *Granzyme B*, emphasizing their cytotoxic capacity. *Klrc1*⁺ cells presented a similar pattern with upregulation of the *Klr* family gene members (*Klkr1*, *Klrc2*), upregulation of the transcription factor *Id2*, the chemokine *Ccl5* and granzyme A and B. Compared to other treatments, PDOX treatment triggered the highest increase of *Klkr1*⁺, *Klrc1*⁺ and *Cxcr3*⁺ cells (**Figure 3A**).

The gene product of *Klkr1*, NKG2D, is known as a molecule with the capacity to provide costimulatory signals to T cells, whereas NKG2A is identified as an inhibitory receptor. Blockade of NKG2D could thus alleviate the positive effect of PDOX treatment on tumor control. To interrogate this hypothesis, we designed *in vivo* experiments in which blockade of NKG2D, using neutralizing antibodies, was combined with PDOX treatment (**Figure 3B**). Whereas NKG2D blockade by itself had no consequence, the effectivity of the PDOX treatment on controlling tumor outgrowth was reduced by the addition of the αNKG2D blocking antibodies (**Figure 3C**). Remarkably, αNKG2D blockade combined with PDOX treatment did not affect the number of CD43⁺ CD8⁺ T cells or tumor antigen-specific CD8⁺ T cells in the blood but the effect of αNKG2D blockade related to a diminution of CD43⁺ CD8⁺ T cells in the tumor-micro-environment. Thus, αNKG2D blockade seem to interfere with recruitment of effector T cells into the TME. To test whether blocking of adhesion receptors expressed on the CD43⁺ subset had similar effects we blocked the chemokine receptor CXCR3. Blockade of CXCR3 using blocking antibodies resulted in lower CD43⁺ CD8⁺ T cells in the TME while the CD43⁺ CD8⁺ T cells and tumor-specific CD8⁺ T cells even accumulated in the blood (**Figure 3D and 3E**).

Early effector T cell response kinetics as predictors for immunotherapy

To gain insight into the dynamics of the therapy-responsive T cell subsets, we longitudinally followed the CD43⁺ T cells in the blood of tumor-bearing mice. Anti-OX40/CpG treatment but not αPD-L1 treatment increased the CD43⁺CD8⁺ T cell subset at day 13 post-tumor challenge. PDOX treatment however resulted in a further amplification of the CD43⁺CD8⁺ T cells, which peaked at day 18 post-tumor challenge (**Figure 4A**). In non-tumor bearing mice, anti-OX40/CpG and PDOX treatment increased the CD43⁺CD8⁺ T cells similarly, indicating that the synergy between anti-OX40/CpG and αPD-L1 blockade to induce the effective treatment-associated T cells is likely driven by the tumor. The kinetics of the CD43⁺ CD8⁺ T cells achieved its peak already thirteen days after tumor challenge. Also here, PDOX treatment induced the highest level of CD43⁺ CD4⁺ T cells compared to other treatment groups (anti-OX40/CpG, αPD-L1) and untreated mice. These higher

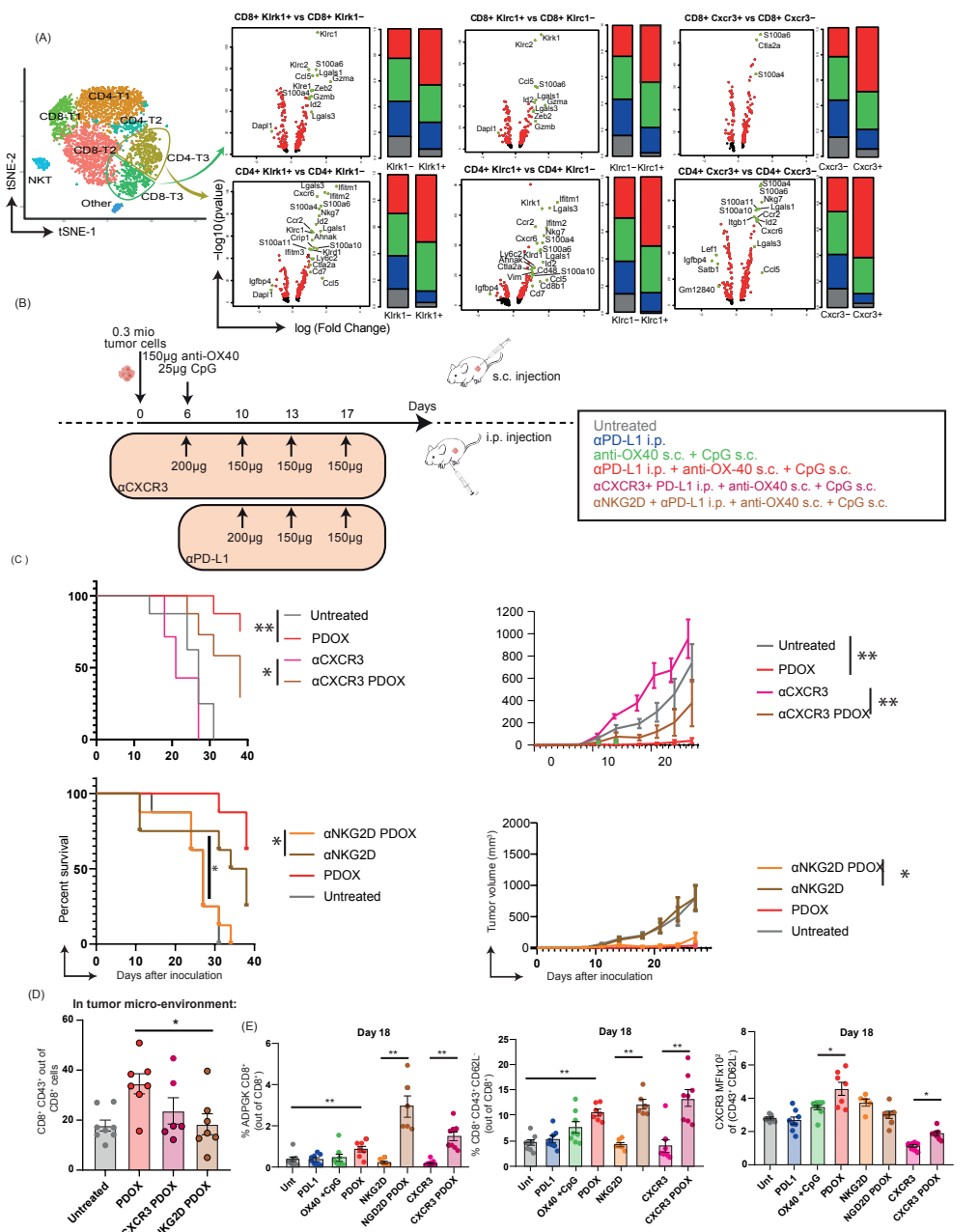


Figure 3. (A) Volcano plots from gated Klrk1+, Klrc1+, Cxcr3+ from either CD4 or CD8 T cells identified on the tSNE map, illustrating the log₂ fold change (FC) in gene expression on the x-axis and unadjusted P values from Student t tests on the y-axis between the groups indicated above each plot. A bar graph represents the percentage of the cell origin according to their group (Untreated in grey, PD-L1 in blue, OX40 in green or PDOX in red). Black points: genes with adjusted P-value > 0.05, red points: genes with adjusted P-value < 0.05 and absolute average log₂ Fold-Change < 1, green points with gene name label: genes with adjusted P-value < 0.05 and absolute average log₂

Fold-Change > 1. (B) Design of the experiment to characterize the kinetics of the CD62L⁻ CD43⁺ T cells. Blood is analyzed 18 days after tumor challenge and mice are treated in four different ways (n=8 per group) as shown. (C) Comparison of the survival and the mean (+/- SEM) of tumor growth between the groups described in (B), n=8 mice per group. (D) Study of the TME after 18 days as indicated on the bar graphs in a sub-optimal treatment (all injections delayed of 2 days). The amount of CD8⁺ CD43⁺ cells are shown and compared between the different groups at day 18, (untreated n=8 mice, PDOX n= 7 mice, CXCR3 PDOX n= 6 mice, NKG2D PDOX n= 7 mice) with the same color code as above displayed on a per-mouse basis with mean +/- SEM. (E) Study of the blood after 18 days. The percentage of ADPGK out of CD8⁺ T cell (%), CD8+ CD43+ CD62L⁻ cell (%), the MFI of CXCR3 and Sca-1 are represented across eight different groups, n=8 mice per group.

CD43⁺ CD4⁺ T cell levels lasted until day 25 and was only observed in tumor-bearing mice (Figure 4B).

To correlate the level of CD43⁺CD8⁺ T cells to tumor progression, the percentage of CD8⁺ CD62L⁻ CD43⁺ was ranked for all groups and the clinical outcome indicated. The vast majority of the mice with a percentage of CD43⁺ CD8⁺ T cells greater than 3% in the blood controlled MC38 tumor outgrowth, whereas none of the mice presenting a percentage of lower than 3% could clear the tumor. This threshold of 3% was even more pronounced in mice challenged with HCMel12 tumors. Altogether, these data suggest that specific effector T cell subsets expand and contract, and this phenomenon correlates to tumor immunity (Figure 4C). Similar results could be determined while studying the expression of Sca-1 on CD8⁺ CD43⁺, correlating with tumor immunity as well (Figure 4D).

System-wide characterization of immunotherapy-responsive T cell subsets by CyTOF

To interrogate the system-wide effect of effective ICT, we dissected the blood and other lymphoid compartments including the spleen, bone marrow, lymph nodes by mass cytometry (Figure 5A). We developed a 38-marker panel based on our previous data sets including the markers CD43, Sca-1, KLRG-1 (Figure S4A). As anticipated, in the blood compartment clusters expressing CD43 are more abundant in the PDOX treated group compared to other groups (16.3 % for PDOX, < 8.6% for other groups) (Figure 5B). Moreover, certain clusters (e.g. cluster CD8-11) are co-expressing markers like CD38, CD39, CD54, KLRG1, and NKG2A. The spleen also contained CD8⁺ T cells co-expressing CD43 and other activation markers upon PDOX treatment (cluster 8, PDOX: 5%, others: less than 1%). The lymph node compartment contained more CD43⁺ICOS⁺CD38⁺ CD4⁺ T cells in the PDOX group. In the bone marrow two CD43⁺ CD4⁺ T cell subsets were identified as more abundant upon efficient therapy (18% in PDOX vs < 11% in other therapies), and these cells co-expressed PD-1, LAG-3, ICOS and CD54.

Next, we integrated the identified immune cell clusters across all tissues in one immune-systemwide analysis to highlight the correlation between all subsets

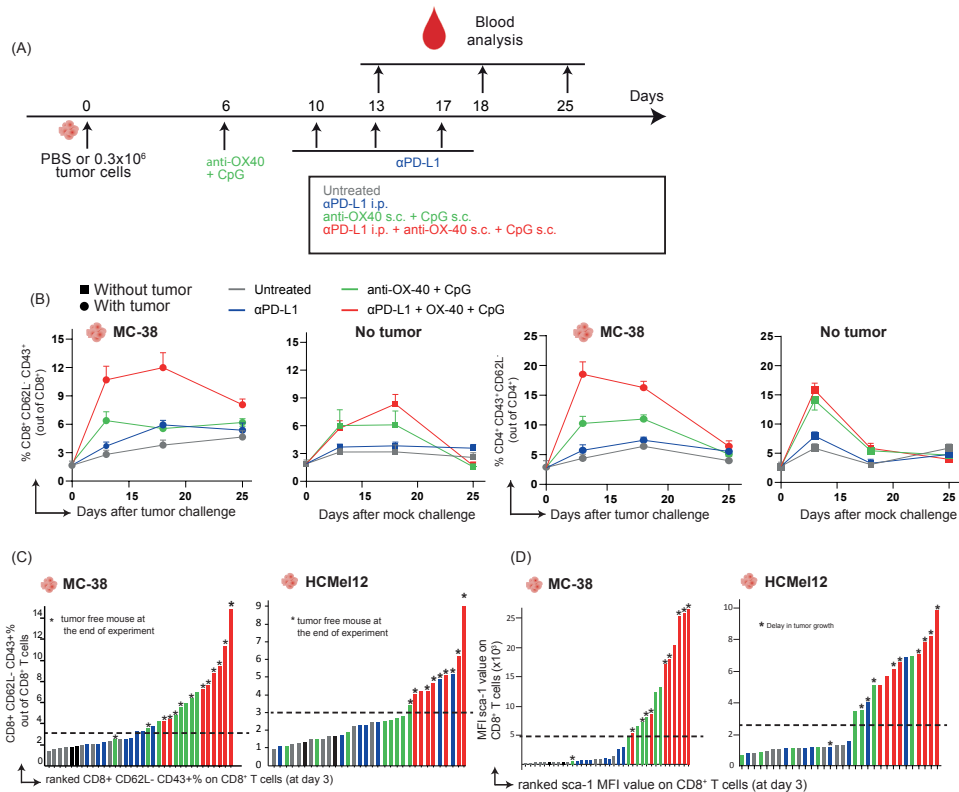


Figure 4. Kinetic study of a CD62L⁻ CD43⁺ subset and correlation with tumor free survival mice. (A) Design of the experiment to characterize the kinetics of the CD62L⁻ CD43⁺ T cells. Blood is analyzed 13 and 18 days after tumor challenge and mice are treated in four different ways (n=8 per group) as shown, naïve mice showing a percentage CD62L⁻ CD43⁺ T cells at Day 13 below 1%. (B) Kinetics of the CD43⁺ T cells across days at three different timepoints (13, 18 and 25 days after tumor injection) investigated by flow cytometry according to their treatment anti-PD-L1 (blue), anti-OX40 (green), combination (red) treatment or if left untreated (grey). Mice are either injected with tumor (round symbol) or left without tumors (square symbols). (C) Correlation between tumor-free rate and CD62L⁻ CD43⁺ T cell percentage at Day 25 for each individual MC38-bearing-mice (left panel) or HCMel12-bearing-mice (right panel). (D) Correlation between tumor-free rate and Sca-1 expression on CD62L⁻ CD43⁺ T cell percentage at Day 25 for each individual MC38-bearing-mice (left panel) or HCMel12-bearing-mice (right panel).

(Figure 5B). Spearman correlation revealed the relationships between the immune cell subsets in the tissues. The therapy-responsive T cell subsets in the blood are most closely connected to those in the spleen and bone marrow, whereas the lymph node T cell subsets are connected to the spleen. System-wide immunity may thus involve the bone marrow, lymph nodes, spleen and the blood to enable efficient tumor immunity. Altogether, these data show the identification of therapy-responsive effector T cell subsets that are not only existing in the blood compartment but omnipresent in basically all tissues of the immune system.

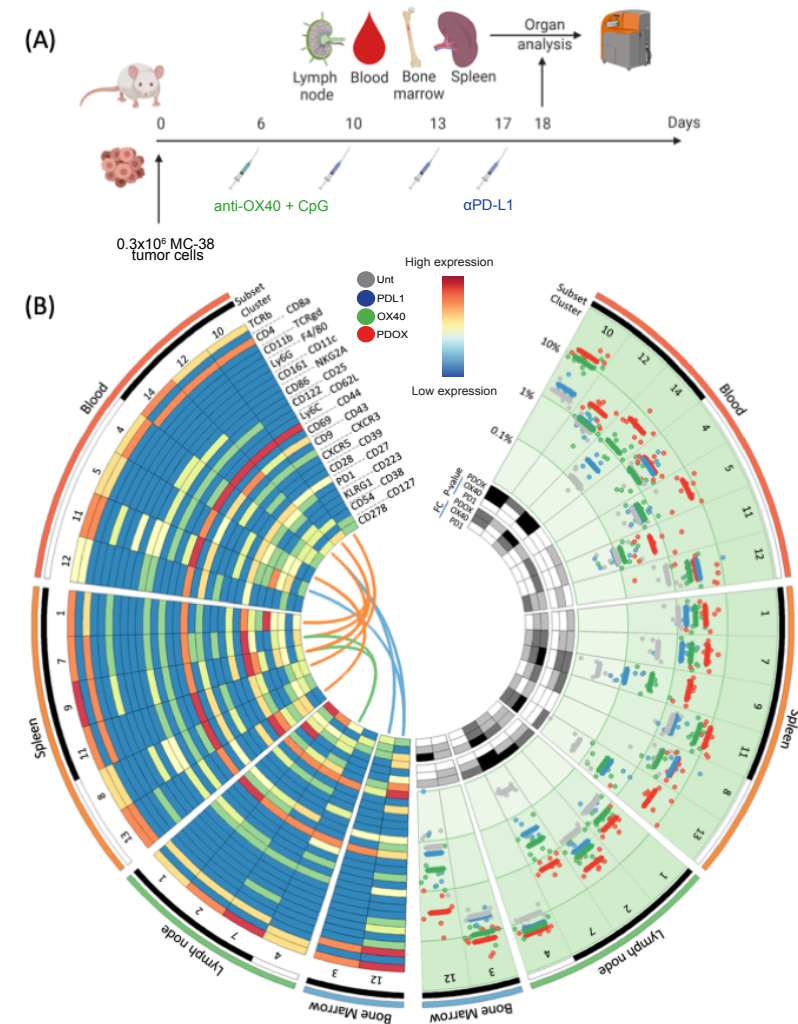


Figure 5. Systemic CyTOF analysis following immunotherapy. (A) Schematic of CyTOF mass cytometry experiment investigating the systemic effect of four different immunotherapies. (B) Circle diagram showing 19 CD4 and CD8 T cell clusters in blood, spleen, lymph nodes or bone marrow. Clusters are mirrored with phenotypic information on the left and abundance in mouse groups on the right. From outside in: CD8 T cell (white bars) and CD4 T cell (black bars) clusters are indicated with cluster number given below. On the left, a heatmap for 32 markers measured by CyTOF depicts normalized expression for each marker per cluster. Clusters that are highly correlated ($r > 0.8$) between compartments are connected by lines, which are colored according to their compartment. On the right, frequency of a subsets within its parent (CD4 or CD8 T cells) is given per cluster on a log-scale. Each dot represents one animal treated with either PDOX (red, n=7-8), OX40 (green, n=8), PD1 (blue, n=5) and untreated (grey, n=5). Mean values per group are indicated by diamonds. Multiple-testing corrected p-values for each of the 3 treated groups compared to the control group are shown, with $p > 0.01$ (white), $p < 0.01$ (light grey), $p < 0.001$ (dark grey), $p < 0.0001$ (black). P-values were based on t-test on log-transformed frequencies and corrected by Benjamini-Hochberg correction. Then means of fold changes (FC) of log-transformed values of groups over the untreated group are shown with $FC < 2$ (white), $FC > 2$ (light grey), $FC > 4$ (dark grey), $FC > 16$ (black).

Systemic immunity is transposable to the human settings in melanoma or NSCLC cancers

We next investigated if the blood compartment could inform on the therapeutic efficacy of immunotherapeutic treatments like PD-1 blockade. We gathered 4 NSCLC (2 responders and 2 non-responders) and 9 melanoma (5 responders and 4 non-responders) cancer patients and added 4 healthy donors in our cohort for a quality check. Blood was collected before treatment and after 2 weeks and analyzed using a 44 mass-cytometry antibody panel (Figure S4B). An analysis of all the detectable CD8⁺ T cell subsets has been performed by HSNE and significant clusters (CTL-24 and -17) are phenotypically described (Figure 6A) and associated with the corresponding abundance of each cluster in the responder and non-responder group (Figure 6B). These two subsets were present

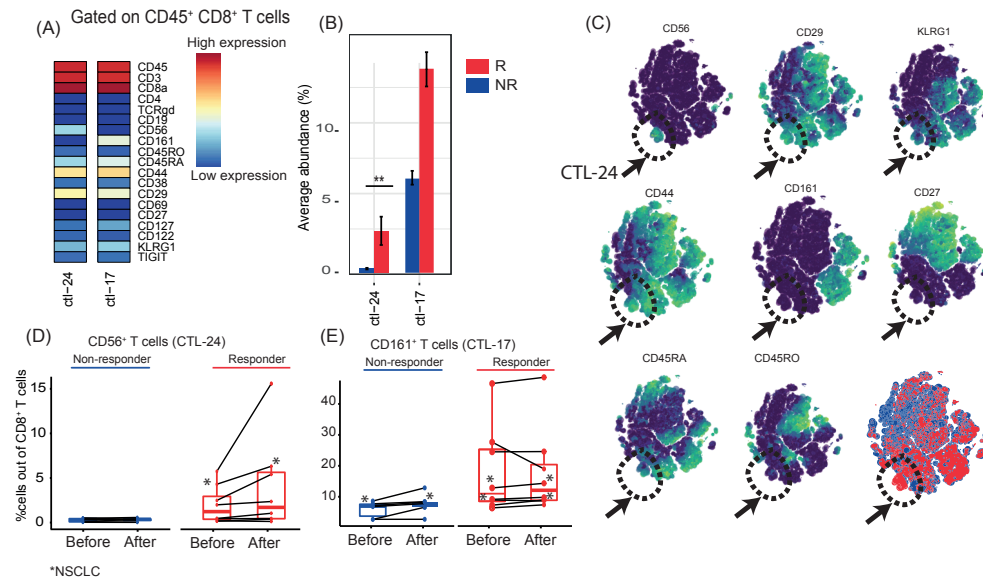


Figure 6. Identification of CD8⁺ T-cell clusters in blood from melanoma patients. (A) Heatmap of all CD8⁺ T-cell clusters identified at baseline or after 2 weeks of PD-1 therapy. Data shown is based on t-SNE plots and is pooled from the responder, non-responder and control groups. Level of ArcSinh5-transformed expression marker is displayed by a rainbow scale. Dendrogram on the top represents the hierarchical similarity between the identified clusters. (B) Average and SEM in percentage of each CD8⁺ T-cell cluster among the CD8⁺ T-cell population of control (blue bars), responder (green bars) and non-responder group (red bars). (C) Bar graph showing the mean frequency of cluster CTL-24 (\pm SEM, paired t-test on the left panel; unpaired t-test on the right panel) between before and after PD-1 therapy for both responder (green) and non-responder (red) groups. (D) Bar graph showing the mean frequency of specifically mentioned CD161⁺ T cell clusters (\pm SEM, paired t-test) comparing responder (green) and non-responder (red) groups. (E) Bar graph showing the mean frequency of specifically mentioned CD161⁺ T cell clusters (\pm SEM, unpaired t-test) comparing healthy donor (blue), responder (green) and non-responder (red) groups. (F) tSNe plot where one dot represents one cell showing the level of expression marker by a rainbow scale from blue to green. The arrow identifies cluster of interest CTL- 24.

in a higher abundance in the responder group compared to the non-responder group. CTL-24 and -17 had the specificity to respectively express CD56 and CD161, making those two markers relevant for immunotherapy screening, a t-SNE map colored per group showed the specificity of CD56 for the responder group (Figure 6C). Over time, within two weeks PD-1 blockade triggered a higher amount of CTL-24 in the responder groups (from 1 to 3%) whereas it remains absent in the non-responder group (Figure 6D). There is however not a specific pattern regarding PD-1 therapeutic effect on the abundance of CD161⁺ cells (Figure 6E), those being more abundant at baseline, correlating with favorable clinical outcome.

DISCUSSION

Immunotherapy has placed itself firmly as an important treatment option amongst conventional therapies such as radiotherapy and chemotherapy in the clinic but oftentimes the clinical responses are partial and variable. Given the substantial variability regarding immunotherapy response, identification of biomarkers in an accessible immune compartment like the blood is necessary to allow for discrimination between responders and non-responders. Such an approach allows tailoring of the treatment to individual patients that are unlikely to respond.

Our work demonstrated a systemic T cell response upon efficient immunotherapy that is characterized by a unique gene and phenotypic signature with similarities to NK cell receptor-expressing T cells that appear upon infection. In two different murine models HCMel12 (uveal melanoma) and MC-38 (colorectal carcinoma), the tumoricidal activity of monotherapy was limited, whereas the combination of an anti-PD-L1 antagonist and an anti-OX40 agonist was exceptionally efficient in eradicating progressing tumors. These data show the importance of using combinatorial treatment of already used therapeutics in patients, i.e. anti-OX40 (24) and anti-PD-L1 (25), and emphasized the potential of this combination as also observed in other mouse tumor models recently (26, 27). The synergic effect of the combinatorial treatment was deciphered by complementary high-dimensional single-cell technology platforms. Both scRNA-seq and mass cytometry highlighted functionally active effector T cell states that were dynamic in their kinetics and characterized by NK receptor expression and expression of adhesion/migration receptors. The kinetics of these effector cells showed an expansion followed by a retraction phase, that is typical for acute infection, and may reflect the temporal activation.

The expression of CD43 on CD8⁺ T cells was a strong marker for these cells as an indicator for effector function based on the co-expression of the NK cell receptors and granzymes. The co-expression of the stemness marker Sca-1 indicated that these cells are antigen-experienced cells (28). In line with our previous findings, it could be suggested that those cells are in a proliferative state and correspond in the tumor environment to a T_{A1} cell phenotype as described recently (29, 30). Interestingly in humans, mass cytometry analysis revealed that the CD62L^{low} CD4⁺ T cell subset expressed T-bet⁺ and CXCR3⁺, indicative of a Th1 subpopulation (31). These results are also in line with our functional

study, which identified the importance in tumor immunity of the Klr family genes, among them NKG2D, but also chemokines like CXCR3.

Our study indicated that the efficiency of immunotherapeutic treatment is mirrored by the induction of specific peripheral T cells. Here, we identified several markers on CD8⁺ T cells in the blood, of which some are closely linked to the effectiveness of immunotherapy. For example, ICOS is one of the upregulated molecules upon PDOX treatment, and this marker is linked to effective immunotherapy in mice (32) but also in responsive patients (33).

Altogether, we have provided evidence for an effective-related-treatment immune signature. Future studies entailing a systematic and multicenter cohort of patients with different cancer types for which a PDOX treatment is approved remains needed. A prediction signature might then be directly used in clinical practice to stratify different levels of effectiveness of treatments.

CONTRIBUTIONS

GB conceived the study, performed the experiments, analyzed the data and wrote the manuscript. EvdG, TW, EBN, MC, SvD and MC helped with tumor material processing and animal experiments. TA provided sc-RNA-sequencing analysis. RA designed the experiments, initiated and supervised the project and wrote the manuscript. FO reviewed the manuscript and provided scientific advice. All authors discussed the results and commented the manuscript. All authors read and approved the final manuscript.

ACKNOWLEDGMENT

We would like to thank Camilla Labrie and Iris Pardieck for their technical support in performing animal experiments and CyTOF processing, and the LUMC flow cytometry facility for their support during CyTOF acquisition.

FUNDING

The authors acknowledge funding from the European Commission (Horizon 2020 MSCA grant under proposal number 675743; project acronym ISPIC) and from the Dutch Cancer Society (UL 2015–7817).

REFERENCES

1. Spitzer MH, Carmi Y, Reticker-Flynn NE, Kwek SS, Madhireddy D, Martins MM, et al. Systemic Immunity Is Required for Effective Cancer Immunotherapy. *Cell*. 2017;168(3):487-502 e15.
2. Galon J, Costes A, Sanchez-Cabo F, Kirilovsky A, Mlecnik B, Lagorce-Pages C, et al. Type, density, and location of immune cells within human colorectal tumors predict clinical outcome. *Science*. 2006;313(5795):1960-4.
3. Pardoll DM. The blockade of immune checkpoints in cancer immunotherapy. *Nat Rev Cancer*. 2012;12(4):252-64.
4. Robert C, Schachter J, Long GV, Arance A, Grob JJ, Mortier L, et al. Pembrolizumab versus ipilimumab in Advanced Melanoma. *N Engl J Med*. 2015;372(26):2521-32.
5. Robert C, Ribas A, Schachter J, Arance A, Grob JJ, Mortier L, et al. Pembrolizumab versus ipilimumab in advanced melanoma (KEYNOTE-006): post-hoc 5-year results from an open-label, multicentre, randomised, controlled, phase 3 study. *Lancet Oncol*. 2019;20(9):1239-51.
6. Benedict CA, Ware CF. Virus targeting of the tumor necrosis factor superfamily. *Virology*. 2001;289(1):1-5.
7. Infante JR, Hansen AR, Pishvaian MJ, Chow LQM, McArthur GA, Bauer TM, et al. A phase Ib dose escalation study of the OX40 agonist MOXR0916 and the PD-L1 inhibitor atezolizumab in patients with advanced solid tumors. *Journal of Clinical Oncology*. 2016;34(15_suppl):101-.
8. Gubin MM, Zhang X, Schuster H, Caron E, Ward JP, Noguchi T, et al. Checkpoint blockade cancer immunotherapy targets tumour-specific mutant antigens. *Nature*. 2014;515(7528):577-81.
9. Newell EW, Sigal N, Nair N, Kidd BA, Greenberg HB, Davis MM. Combinatorial tetramer staining and mass cytometry analysis facilitate T-cell epitope mapping and characterization. *Nat Biotechnol*. 2013;31(7):623-9.
10. Hartmann FJ, Babdor J, Gherardini PF, Amir ED, Jones K, Sahaf B, et al. Comprehensive Immune Monitoring of Clinical Trials to Advance Human Immunotherapy. *Cell Rep*. 2019;28(3):819-31 e4.
11. Subrahmanyam PB, Dong Z, Gusenleitner D, Giobbie-Hurder A, Severgnini M, Zhou J, et al. Distinct predictive biomarker candidates for response to anti-CTLA-4 and anti-PD-1 immunotherapy in melanoma patients. *J Immunother Cancer*. 2018;6(1):18.
12. Krieg C, Nowicka M, Guglietta S, Schindler S, Hartmann FJ, Weber LM, et al. High-dimensional single-cell analysis predicts response to anti-PD-1 immunotherapy. *Nat Med*. 2018.
13. Gubin MM, Esaulova E, Ward JP, Malkova ON, Runci D, Wong P, et al. High-Dimensional Analysis Delineates Myeloid and Lymphoid Compartment Remodeling during Successful Immune-Checkpoint Cancer Therapy. *Cell*. 2018.
14. Manjarrez-Orduno N, Menard LC, Kansal S, Fischer P, Kakrecha B, Jiang C, et al. Circulating T Cell Subpopulations Correlate With Immune Responses at the Tumor Site and Clinical Response to PD1 Inhibition in Non-Small Cell Lung Cancer. *Front Immunol*. 2018;9:1613.
15. Nixon AB, Schalper KA, Jacobs I, Potluri S, Wang IM, Fleener C. Peripheral immune-based biomarkers in cancer immunotherapy: can we realize their predictive potential? *Journal for ImmunoTherapy of Cancer*. 2019;7(1):325.
16. Takeuchi Y, Tanemura A, Tada Y, Katayama I, Kumanogoh A, Nishikawa H. Clinical response to PD-1 blockade correlates with a sub-fraction of peripheral central memory

1

2

3

4

5

6

7

&

- CD4+ T cells in patients with malignant melanoma. *Int Immunol.* 2018;30(1):13-22.
17. Sade-Feldman M, Yizhak K, Bjorgaard SL, Ray JP, de Boer CG, Jenkins RW, et al. Defining T Cell States Associated with Response to Checkpoint Immunotherapy in Melanoma. *Cell.* 2018;175(4):998-1013.e20.
 18. Spitzer MH, Gherardini PF, Fragiadakis GK, Bhattacharya N, Yuan RT, Hotson AN, et al. IMMUNOLOGY. An interactive reference framework for modeling a dynamic immune system. *Science.* 2015;349(6244):1259425.
 19. Corbett TH, Griswold DP, Jr., Roberts BJ, Peckham JC, Schabel FM, Jr. Tumor induction relationships in development of transplantable cancers of the colon in mice for chemotherapy assays, with a note on carcinogen structure. *Cancer Res.* 1975;35(9):2434-9.
 20. Sagiv-Barfi I, Czerwinski DK, Levy S, Alam IS, Mayer AT, Gambhir SS, et al. Eradication of spontaneous malignancy by local immunotherapy. *Science translational medicine.* 2018;10(426):eaan4488.
 21. Kilian MM, Loeffler KU, Pfarrer C, Holz FG, Kurts C, Herwig MC. Intravitreally Injected Hcmel12 Melanoma Cells Serve as a Mouse Model of Tumor Biology of Intraocular Melanoma. *Curr Eye Res.* 2016;41(1):121-8.
 22. Omilusik KD, Nadjombati MS, Shaw LA, Yu B, Milner JJ, Goldrath AW. Sustained Id2 regulation of E proteins is required for terminal differentiation of effector CD8(+) T cells. *J Exp Med.* 2018;215(3):773-83.
 23. Hernandez JD, Nguyen JT, He J, Wang W, Ardman B, Green JM, et al. Galectin-1 binds different CD43 glycoforms to cluster CD43 and regulate T cell death. *J Immunol.* 2006;177(8):5328-36.
 24. Wang R, Gao C, Raymond M, Dito G, Kabbabe D, Shao X, et al. An Integrative Approach to Inform Optimal Administration of OX40 Agonist Antibodies in Patients with Advanced Solid Tumors. 2019.
 25. Brahmer JR, Tykodi SS, Chow LQ, Hwu WJ, Topalian SL, Hwu P, et al. Safety and activity of anti-PD-L1 antibody in patients with advanced cancer. *N Engl J Med.* 2012;366(26):2455-65.
 26. Messenheimer DJ, Jensen SM, Afentoulis ME, Wegmann KW, Feng Z, Friedman DJ, et al. Timing of PD-1 Blockade Is Critical to Effective Combination Immunotherapy with Anti-OX40. *Clin Cancer Res.* 2017.
 27. Ma Y, Li J, Wang H, Chiu Y, Kingsley CV, Fry D, et al. Combination of PD1 Inhibitor and OX40 Agonist Induces Tumor Rejection and Immune Memory in Mouse Models of Pancreatic Cancer. *Gastroenterology.* 2020.
 28. Kaech SM, Hemby S, Kersh E, Ahmed R. Molecular and functional profiling of memory CD8 T cell differentiation. *Cell.* 2002;111(6):837-51.
 29. Li H, van der Leun AM, Yofe I, Lubling Y, Gelbard-Solodkin D, van Akkooi ACJ, et al. Dysfunctional CD8 T Cells Form a Proliferative, Dynamically Regulated Compartment within Human Melanoma. *Cell.* 2019;176(4):775-89.e18.
 30. Beyrend G, van der Gracht E, Yilmaz A, van Duikeren S, Camps M, Höllt T, et al. PD-L1 blockade engages tumor-infiltrating lymphocytes to co-express targetable activating and inhibitory receptors. *Journal for ImmunoTherapy of Cancer.* 2019;7(1):217.
 31. Kagamu H, Kitano S, Yamaguchi O, Yoshimura K, Horimoto K, Kitazawa M, et al. CD4+ T-cell immunity in the peripheral blood correlates with response to anti-PD-1 therapy. 2019:canimm.0574.2019.
 32. Beyrend G, van der Gracht E, Yilmaz A, van Duikeren S, Camps M, Hollt T, et al. PD-L1 blockade engages tumor-infiltrating lymphocytes to co-express targetable activating and inhibitory receptors. *J Immunother Cancer.* 2019;7(1):217.
 33. Friedman CF, Postow MA. Emerging Tissue and Blood-Based Biomarkers that may Predict Response to Immune Checkpoint Inhibition. *Curr Oncol Rep.* 2016;18(4):21.
 34. Butler A, Hoffman P, Smibert P, Papalexi E, Satija R. Integrating single-cell transcriptomic data across different conditions, technologies, and species. *Nat Biotechnol.* 2018;36(5):411-20.
 35. van der Maaten L, Hinton, G. Visualizing Data using t-SNE. *Journal of Machine Learning Research.* 2008.

1

2

3

4

5

6

7

&

ADDITIONAL FILE

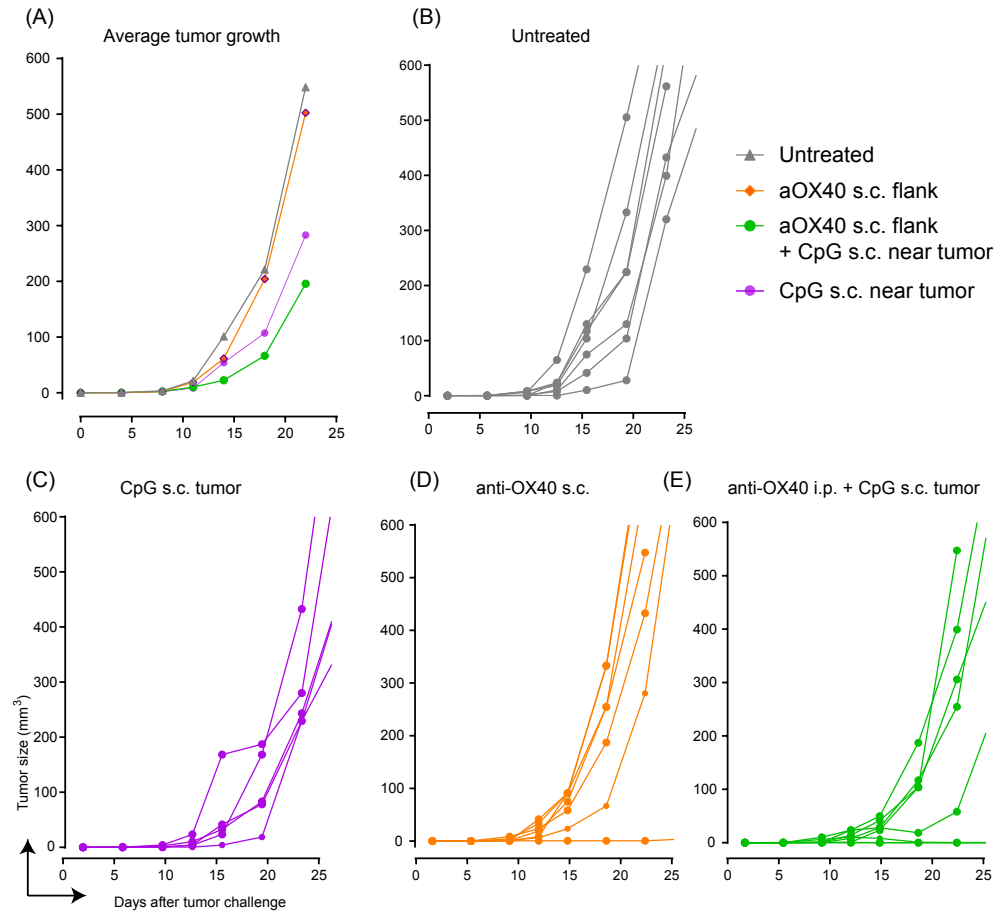


Figure S1. (A) Average of tumor growth of mice different treatments. (B) Tumor growth of individual mice left untreated. (C) Tumor growth of individual mice treated with CpG only near the tumor subcutaneously. (D) Tumor growth of individual mice treated with anti-OX40 only near the tumor subcutaneously. (E) Tumor growth of individual mice treated with anti-OX40 and CpG near the tumor subcutaneously.

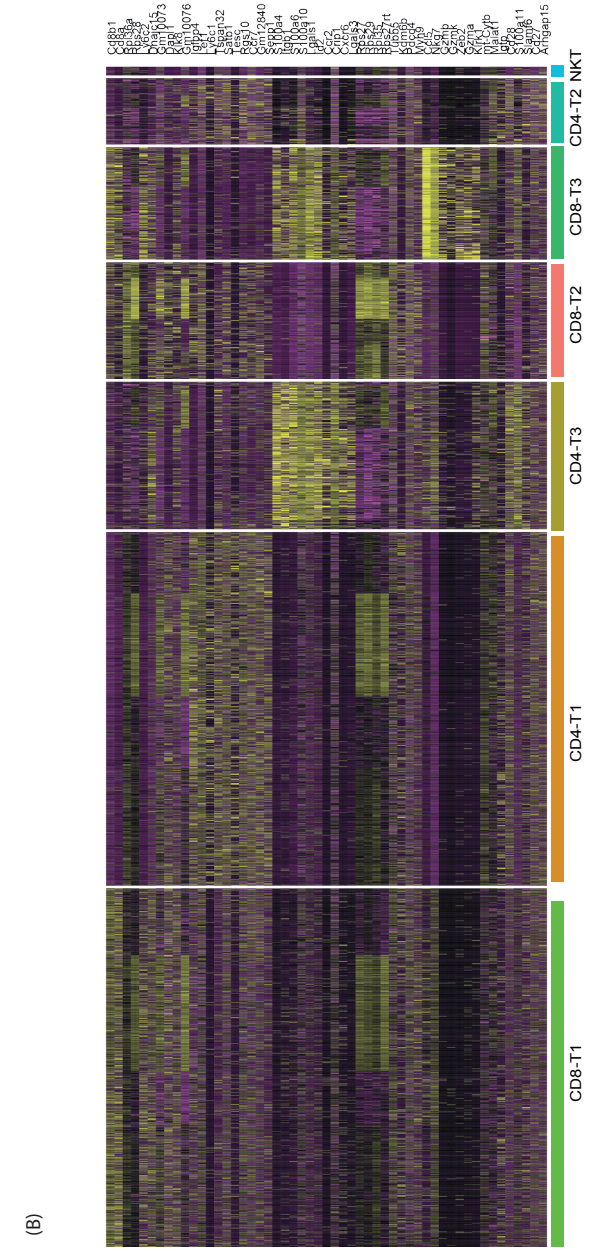


Figure S2. Volcano plots of single cell RNA-sequencing analysis showing high co-expression of Id2 and Lgals1 in T3 subset.

- 1
- 2
- 3
- 4
- 5
- 6
- 7
- &

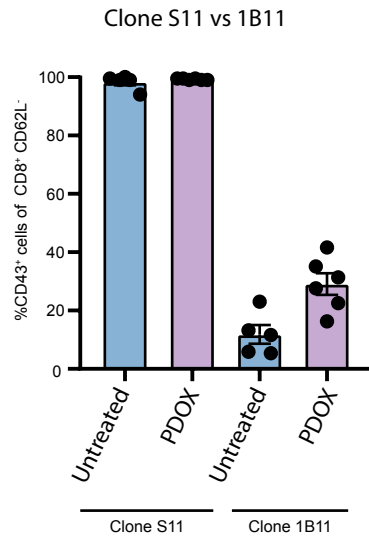


Figure S3. Flow cytometry panels. (A) Flow cytometry panel consisting of 11 extracellular markers to analyze mouse blood. (B) Flow cytometry panel consisting of 8 extracellular markers and 2 tetramers to analyze mouse blood. (C) Flow cytometry panel consisting of 8 extracellular and 2 intracellular markers to analyze mouse tumor-micro-environment. (D) CD43 positive cells in percentage found in the blood at day 18 after PDOX treatment or left untreated, n= 6 mice per group.

Mouse panel		
Antigen	Clone	Company
CD3e	145-2C11	eBiosciences
CD4	RMA45	Fluidigm
CD8A	53-6.7	Fluidigm
CD9	eBioKMC8	eBiosciences
CD11B	M1/70	Fluidigm
CD11C	N418	eBiosciences
CD14	Sa14-2	BioLegend
CD19	6D5	Fluidigm
CD25	3C7	Fluidigm
CD27	LG.3A10	eBiosciences
CD28	37.51	Fluidigm
CD38	90	eBiosciences
CD39	24DMS1	eBiosciences
CD43	1B11	BioLegend
CD44	IM7	eBiosciences
CD45	30-F11	Fluidigm
ICAM-1	YN1/1.7.4	BioLegend
L-selectin	MEL-14	BioLegend
CD69	H1.2F3	Fluidigm
B7-2	GL-1	eBiosciences
C-FMS	AFS98	Fluidigm
CD122	TM-b1	BioLegend
CD127	A7R34	Fluidigm
NK1.1	PK136	eBiosciences
CXCR3	CXCR3-173	eBiosciences
CXCR5	L138D7	BioLegend
LAG-3	eBioC9B7W	eBiosciences
PDL1	10F.9G2	BioLegend
ICOS	7E.17G9	BioLegend
PD1	29F.1A12	eBiosciences
F4/80	BM8	eBiosciences
KLRG1	2F1	eBiosciences
Ly6C	HK1.4	eBiosciences
Ly6G	1A8	Fluidigm
MHC II	M5/114.15.2	eBiosciences
NKG2A	20d5	eBiosciences
TCRab	H57-597	BioLegend
TCRgd	eBioGL3	eBiosciences

Human panel		
Antigen	Clone	Company
CD38	HIT2	BioLegend
CD45RO	UCHL1	Fluidigm
CD45RA	HI100	BioLegend
CD44	IM7	Fluidigm
CD45	HI30	Fluidigm
CD49b	P1E6-C5	BioLegend
CD39	A1	BioLegend
HLA-DR	L243	Fluidigm
CD29	TS2/12	BioLegend
CD11b (Mac-1)	ICRF44	Fluidigm
TCRgd	11F2	Dianova
CD274 (PD-L1)	29E.2A3	Fluidigm
CD8a	RPA-T8	Fluidigm
CD278/ICOS	C398.4A	Fluidigm
CD103	Ber-ACT8	BioLegend
CD49A	SR84	BD Biosciences
CD27	L128	Fluidigm
CD127 (IL-7Ra)	A019D5	Fluidigm
CD25 (IL-2R)	2A3	Fluidigm
CD3	UCHT1	Fluidigm
CD4	RPA-T4	Fluidigm
TIGIT	MBSA43	eBioscience
CXCR5	MAB190	RnDsystems
CD62L	DREG-56	BioLegend
CD69	FN50	BioLegend
CD86	IT2.2	Fluidigm
CD154 (CD40L)	24-31	ThermoFischer
CD134 (OX40)	ACT35	BD Biosciences
CD161	HP-3G10	Fluidigm
CD335 (NKp46)	BAB281	Fluidigm
KLRG1	SA231A2	BioLegend
CD223/LAG-3	11C3C65	Fluidigm
CD20	2H7	BioLegend
CD14	Tük4	ThermoFischer
CD56	5.1H11	BioLegend
CD150	A12	BioLegend
CD244	2-69	BioLegend
CD160	BY55	BioLegend
CCR6	GE034E3	BioLegend
CD122	Tu27	BioLegend
4-1BB	4B4-1	BioLegend
CXCR6	KE041E5	BioLegend
NKG2A	131411	RnDsystems
PD-1	EH12.2H7	Fluidigm

Figure S4. Mass cytometry panels. (A) Mouse cytometry panel used to analyze the blood, spleen, lymph nodes and bone marrow from mice. (B) Human mass cytometry panel used to analyze the blood of patients or healthy controls. Figure S4: sc-RNA-seq recap

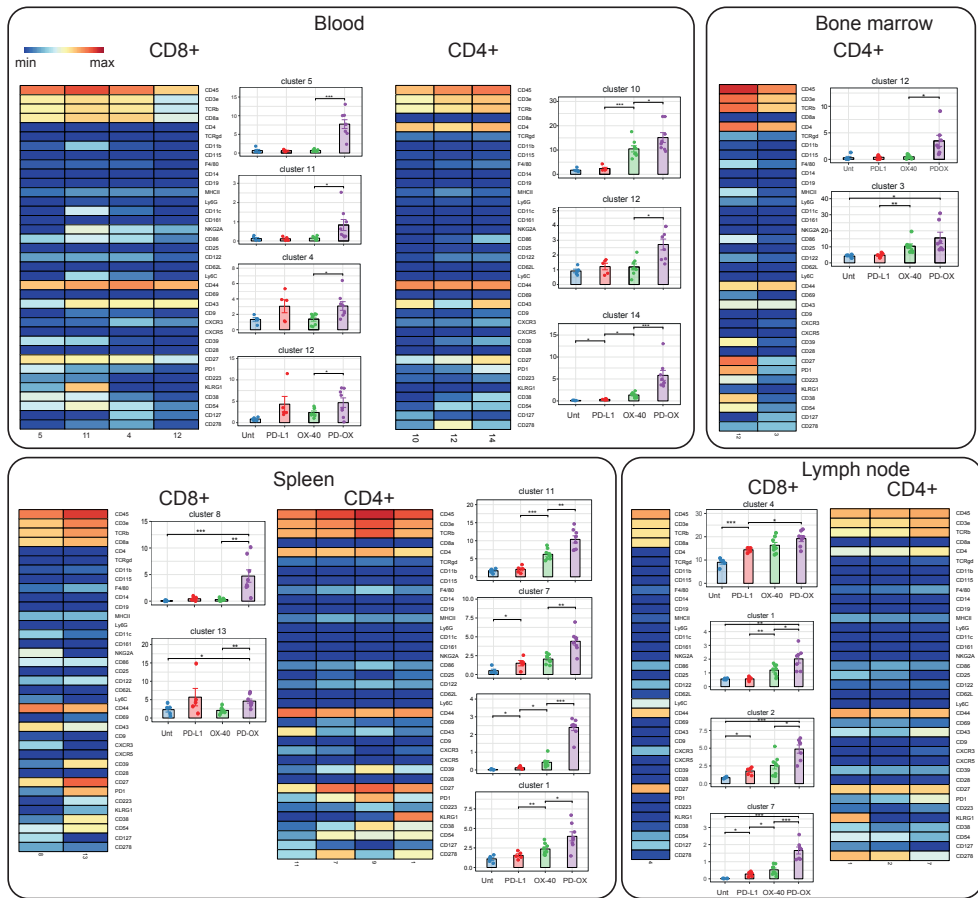


Figure S5.